LU-TP 20-39
July 2020

On the Entropy of Jets

Eivind H. Jørstad

Department of Astronomy and Theoretical Physics, Lund University

Bachelor thesis supervised by Stefan Prestel and Roman Pasechnik

LUND
UNIVERSITY

Abstract

High energy particle collisions often produce large numbers of partons in the final state, which are clustered together in collimated sprays called jets. A recent paper [1] introduces the concept of jet entropy, which is an observable that quantifies the entanglement between the resolved and unresolved parts of a jet. We derive an analytic expression for the entropy of a gluon jet and compare the result to that of a simple event generator. Our results show that jet entropy is sensitive to the treatment of recoil, which suggests a novel way of testing recoil prescriptions against experimental data. We also examine models of graviton jets where the splitting functions are obtained by removing collinear pieces from gluon splitting functions, and find that the entropy depends strongly on how the collinear pieces are removed.

Acknowledgements

I would like to thank my supervisors Dr. Stefan Prestel and Dr. Roman Pasechnik for their guidance during this project. I am also grateful to Santiago Londoño Castillo for many interesting and helpful discussions.

Eivind H. Jørstad

Popular description

Everything we see around us is built from the same set of fundamental building blocks, called elementary particles. Two interesting groups of such particles are the *quarks* and *gluons*, which are found inside the nuclei of atoms. Just like electrons carry electrical charge, quarks and gluons carry a so-called color charge, and the theory that describes their interactions is called *quantum chromodynamics* (QCD).

In QCD, the forces between quarks are mediated by gluons, like how two astronauts floating in space can exert a force on each other by passing a basketball back and forth. (Note that the forces can be attractive, which this analogy does not capture.) Interestingly, quarks are never observed as free particles – the gluons always keep them bound together in groups. Such groups of quarks are particles in their own right, and they include well known examples like the proton and the neutron.

If we try to separate a group of quarks, we will always create additional particles in the process. This can be understood by imagining a piece of elastic string, where the endpoints represent quarks and the string represents gluons. If we try to separate the quarks, we must pull the string, which at some point breaks. The break creates two new string-endpoints, which represent two new quarks. Now, in a high energy particle collision, the elastic strings can be broken several times over, so a large number of particles are created. These particles will travel outwards from the collision site in clusters called *jets*. Jets contain information about the initial collision, so they are important objects to study.

In this thesis we calculate the entropy of a jet, which roughly tells us how much information about the jet is carried away by particles that are not registered in our experiments. We do this for jets consisting of gluons, as well as jets consisting of gravitons, which are the particles that mediate the gravitational force. Our conclusion is that by studying the entropy of jets, we can learn something about how to make better computer simulations of QCD.

Contents

1 Introduction

In particle collider experiments, interactions are studied by observing the final state remnants, which often include large numbers of partons arranged in collimated sprays called *jets*. In addition to common jet observables like particle multiplicity and jet mass, a recent paper by Neill and Waalewijn [1] shows that we can also measure a jet entropy, defined as the entanglement entropy between resolved and unresolved partons. (See section 3.1 for a more detailed definition.) In that paper, they derive an analytic expression for jet entropy and compare it to numerical calculations, where recoil effects are ignored.

In this thesis, we develop a simple event generator based on [2] in order to test how recoil affects the jet entropy, and find a significant effect at high resolutions. Due to this sensitivity to recoil, we suggest that jet entropy can be used to test different recoil prescriptions against experimental data, which has previously been challenging. Our event generator uses transverse momentum as its evolution variable, and our results can therefore not be directly compared to those of Neill and Waalewijn, who order their jets by emission angle. Instead, we compare our numerical result to an analytic expression for the entropy of transverse momentum ordered jets, which we derive by solving a modified version of an equation presented in [1].

Similarly to gluons, the gravitons of perturbative quantum gravity are massless and self-coupling. However, graviton radiation does not produce hard collinear singularities due to their spin-2 structure and energy-momentum conservation. (A derivation of this fact can be found in [3].) Therefore, we attempt to model the graviton splitting kernels by removing collinear pieces from the gluon kernels and ignoring color factors. We test how the different graviton splitting kernels affect the structure and entropy of the jet, and find that the entropy depends strongly on the choice of collinear piece.

This thesis is divided into five main parts. First, in section 2 we use calculations in quantum electrodynamics (QED) to motivate the concepts of splitting functions and Sudakov form factors, which will be used extensively in later sections. After that, we derive the entropy of a gluon jet in section 3. In section 4 we explain our event generator, and in section 5 we show its results for the gluon and graviton splitting functions. Finally, in section 6 we make some concluding remarks and discuss possible further work.

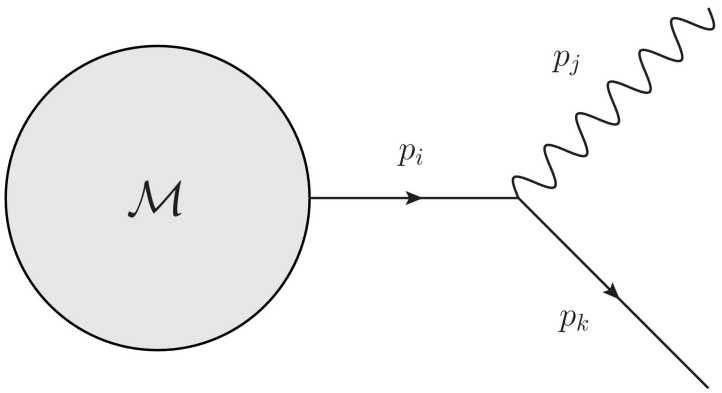

Figure 1: An arbitrary interaction followed by radiation of a photon from an otherwise external electron leg.

2 Splitting and singularities

In this section we discuss splitting probabilities and how they relate to the cancellation of infrared singularities. In particular, we carry out a derivation of an $e \to \gamma e$ splitting function in QED. We also discuss the appearance of a Sudakov form factor in the splitting probability due to the ordering of emissions. These calculations should be considered as analogies to similar concepts in QCD, which will be used to calculate the entropy of a gluon jet in section 3 and which form the basis for our event generator in section 4. Although we carry out these derivations in QED, we will restrict ourselves to discussing gluon (and graviton) jets from section 3 onward. This is because the analytic expression for jet entropy is only readily derivable for self-coupling bosons.

2.1 Splitting functions

In general terms, a splitting function $P_{i\to jk}(z)$ gives the probability that a particle i splits into the particles j and k, each carrying a fraction z or $1-z$ of the original energy. Splitting functions appear naturally in the following way: In the collinear limit $p_j \parallel p_k$ of a process like in Fig. 1, the cross section factorizes into the cross section of the underlying process and a factor that has unphysical singularities. As per the Kinoshita-Lee-Nauenberg theorem [4], the singularities must be cancelled by instead computing the cross section of a larger set of interaction, usually including virtual contributions. After this has been done, the remaining factor multiplying the non-emission cross section is interpreted as the probability for a splitting to occur, and is called the splitting function of the process.

As a demonstration, consider the process in Fig. 1 in which an outgoing electron radiates a photon. Here, we will derive the splitting function based on chapter 2.8.3 in [5]. In the massless electron limit, we have the matrix element

$$\mathcal{M}^{\text{split}} = \bar{u}_\kappa(p_k) i e \not{\epsilon}^*_\lambda \frac{i\not{p}_i}{p_i^2 + i\varepsilon} \mathcal{A}(p_i, p_a), \tag{2.1}$$

where $\mathcal{A}$ corresponds to the unspecified part of the interaction, p_a represents all the unspecified external momenta, ϵ is the photon polarization vector, u is a Dirac spinor and λ and κ are helicity indices. We parameterize the momenta as in eqs. A.1-A.3, and make the approximation

$$\not{p}_i = \sum_\kappa u_\kappa(p_i)\bar{u}_\kappa(p_i) + \mathcal{O}(p_\perp^2), \tag{2.2}$$

where $p_\perp$ is the transverse momentum of the splitting, defined in the appendix. This gives the matrix element

$$\mathcal{M}^{\text{split}} = \sum_\kappa V_{\text{EM},\kappa\kappa'} \frac{z(1-z)}{p_\perp^2} \mathcal{M}(p_i, p_a) + \mathcal{O}(p_\perp^0), \tag{2.3}$$

where z is the momentum fraction described above and V_{EM} is the electromagnetic vertex. By inserting the explicit form of the spinors in the Weyl representation we get

$$\sum_{\kappa\kappa'} V_{\text{EM},\kappa\kappa'} V^*_{\text{EM},\kappa\kappa'} = 2e^2 \frac{p_\perp^2}{z(1-z)} \frac{1+z^2}{1-z} + \mathcal{O}(p_\perp^4), \tag{2.4}$$

which, after computing the cross section in the standard way and rewriting the phase space element as

$$\frac{\mathrm{d}^3\mathbf{p}_j}{2|\mathbf{p}_j|} \frac{\mathrm{d}^3\mathbf{p}_k}{2|\mathbf{p}_k|} \mathrm{d}^4\mathbf{p}_i \; \delta(p_k + p_j - p_i) = \frac{\mathrm{d}^3\mathbf{p}_j}{2|\mathbf{p}_j|} \frac{\mathrm{d}^3\mathbf{p}_i}{2(1-z)} \cdot \frac{1}{z} + \mathcal{O}(p_\perp^4), \tag{2.5}$$

gives

$$d\sigma^{\text{split}}(p_i) = d\sigma(p_i) \left[\frac{\alpha}{2\pi} \log\left(\frac{p^2_{\perp\max}}{p^2_{\perp\min}} \right) \int_{z_{\min}}^{z_{\max}} dz \frac{1+z^2}{1-z} \right], \tag{2.6}$$

where $p_{\perp\max}$ is the maximal transverse momentum, $p_{\perp\min}$ is an explicit lower cut-off (e.g. due to the electron mass), and $z_{\min}$ and $z_{\max}$ are phase-space limits on the energy fraction due to a non-vanishing transverse momentum. The cross section in eq. 2.6 has factorized into the non-splitting cross section and a factor that diverges when the lower phase space cutoffs go to zero (i.e. when $z_{\min} \to 0$ or $p_{\perp\min} \to 0$). Here, we define the splitting function as the z-dependent part of this factor:

$$P_{e\to e\gamma}(z) = \frac{1+z^2}{1-z}. \tag{2.7}$$

At this point we could add the cross section of a virtual diagram, for example one that cancels the infrared divergence (which would give the splitting function the so called (+)-prescription). However, in later calculations and numerical work we will rather use the

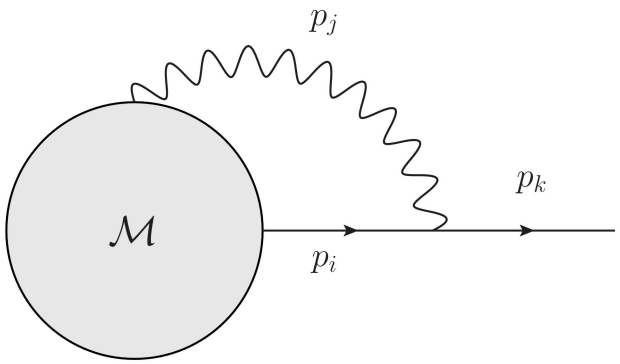

Figure 2: An irreducible virtual diagram. In a transverse gauge this diagram does not contain collinear singularities, and does therefore not contribute to the corresponding splitting function.

splitting function as it appears in eq. 2.7, keeping the phase space cutoffs and including the virtual contributions in an approximate way through the Sudakov form factor (more on this in section 2.2). It is not clear from this calculation that the splitting function is gauge independent. However, note that in a transverse gauge, i.e. a gauge that obeys the condition $N_{\mu\nu}p_j^\nu = 0$ where p_j is the photon momentum and $N_{\mu\nu}$ is the numerator of the photon propagator, there are no collinear singularities coming from irreducible diagrams like the one in Fig. 2. This is because the divergent factor in the matrix element of Fig. 2 is

$$\mathrm{d}\sigma_{\text{virtual}} \propto \frac{N_{\mu\nu}p_i^\nu}{(p_\perp^2)^2}. \tag{2.8}$$

The divergence is slower than $(p_\perp^2)^{-2}$ because $N_{\mu\nu}p_i^\nu \to 0$ in the collinear limit, and therefore disappears when the loop integral over $p_\perp^2$ is performed. The remaining virtual contributions give rise to the plus prescription (see chapter 2.8.3.3 of [5]), and are, as mentioned above, neglected here. There are no remaining diagrams that would affect the splitting probability, and thus our splitting function is gauge independent.

The splitting functions of QCD, known as the Dokshitzer–Gribov–Lipatov–Altarelli–Parisi (DGLAP) splitting functions [6], will be needed in subsequent sections. They are:

$$P_{q\to qg}(z) = C_F\left(\frac{2}{1-z} - (1+z)\right), \tag{2.9}$$

$$P_{g\to gg}(z) = 2C_A\left(\frac{1}{1-z} + \frac{1}{z} - 2 + z(1-z)\right), \tag{2.10}$$

$$P_{g\to qq}(z) = T_R\Big(1 - 2z(1-z)\Big), \tag{2.11}$$

where C_F, C_A and T_R are color factors. A splitting probability in QCD is then given by an expression similar to eq. 2.6, where the term under the z-integral is replaced by a DGLAP splitting function and the electromagnetic coupling constant α is replaced by the

strong coupling constant α_s. Note that the electron-photon splitting function (eq. 2.7) has the same z dependence as the quark-gluon splitting function (eq. 2.9), which might be expected since they both represent the radiation of a massless gauge boson from a fermion leg.

2.2 The Sudakov form factor

In this thesis we assume a leading logarithmic (LL) approximation, in which jets are described by a series of branchings with decreasing transverse momentum. Importantly, this ordered branching gives the dominant contribution to the jet cross section because the propagators are forced to be close to the mass shell. (More on why this gives the dominant contribution can be found for example in chapter 2.3.8.3 of [5]). More physically, such an ordering ensures that we first generate the most resolvable splittings, which would be most relevant experimentally, and then "dress" them with less resolvable particles. In this section, we show the effect of transverse momentum ordering on the splitting probability by treating $p_\perp$ as a kind of "time" (i.e. an evolution variable, which in our case is decreasing in magnitude) following [7], and briefly discuss the physical interpretation of the result.

Without transverse momentum ordering, the probability of a splitting with transverse momentum in the range $R > p_\perp > R'$ is

$$\Gamma(R, R') = \frac{\alpha_s}{2\pi} \int_{z_{\min}}^{z_{\max}} \mathrm{d}z \int_{R'}^{R} \mathrm{d}p_\perp \sum_{j,k} \frac{P_{i\to jk}(z)}{p_\perp}, \tag{2.12}$$

where i denotes the splitting particle and the sum runs over all the possible daughter particles j, k, and where $z_{\max}, z_{\min}$ are phase-space boundaries, to be specified below. The probability of splitting with a given $p_\perp$ is then $(\partial\Gamma/\partial R)\delta R$. However, if the transverse momentum is given the role of an evolution parameter, then a particle of fixed momentum can only split at a given $p_{\perp 2}$ if it has not already split at any $p_{\perp 1} > p_{\perp 2}$. The probability of not splitting at any transverse momentum in the range $R > p_\perp > R'$ is then the product

$$\mathcal{P}_{\text{no-splitting}}(R, R') = \left(1 - \frac{\partial\Gamma}{\partial R}(p_{\perp 1})\delta R\right)\left(1 - \frac{\partial\Gamma}{\partial R}(p_{\perp 2})\delta R\right)\ldots\left(1 - \frac{\partial\Gamma}{\partial R}(p_{\perp n})\delta R\right), \tag{2.13}$$

where we have partitioned the range into n intervals who are ordered like $R > p_{\perp 1} > \ldots > p_{\perp n} > R'$. Note that each factor is an exponential to the first order in δR, so when $\delta R \to 0$ the no-splitting probability turns into an exponential with a Riemann sum in the exponent. The rate at which the no-splitting probability decreases is then equal to the splitting probability, much like in nuclear decay. Thus, we find the probability of splitting with transverse momentum R'

$$\mathcal{P}(R') = -\frac{\partial\mathcal{P}_{\text{no-splitting}}}{\partial R}(R, R') = \frac{\partial\Gamma}{\partial R}(R')\exp[-\Gamma(R, R')], \tag{2.14}$$

where R is the largest allowed value of $p_\perp$, which in the LL approximation is just the transverse momentum of the previous branching in the jet. The exponential factor in eq. 2.14 is known as the Sudakov form factor.

It turns out that eq. 2.14 has a notable physical interpretation. In order to predict the outcome of a given experiment, we must include in our cross sections not only the process we want to study, but also all the similar interactions that contain unresolved particles. These cross sections are accounted for by the Sudakov form factor. That is, it is shown in [3] and [8] that eq. 2.14 is the splitting probability one obtains after including a variety of virtual and real soft contributions to the splitting diagram (see also the discussion in chapter 5 of [9]). For this interpretation to be valid, we must restrict the splitting parameters $p_\perp$ and z to the resolvable region of phase space. In other words, if we do not resolve splittings with energy below $E_{\min}$ and transverse momentum below $R_{\min}$, then we have to set $p_{\perp\min} = R_{\min}$ and $z_{\min} = 1 - z_{\max} = E_{\min}/E$, where E is the energy of the splitting particle.

3 Entropy in QCD

Here, we derive an expression for the entropy of a jet. First, in section 3.1 we show a derivation of a general integral equation for jet entropy based on [1]. Then, in section 3.2 we convert the integral equation into an integro-differential equation for gluon entropy, which is then solved. (Note that the solution of the integro-differential equation is not based on [1], it is our own work.) Our motivation for deriving the analytic entropy is twofold. Firstly, it will allow us to confirm that our numerical results are reasonable. Secondly, since Neill and Waalewijn [1] find excellent agreement between analytic and numerical results by ignoring recoil, any deviations in our results should show the effect of recoil on the jet entropy. Our end goal is then to see whether the entropy is sensitive to recoil, which would suggest this as an interesting observable to consider when different recoil prescriptions are tested against experimental data. The question of why recoil creates deviations between the analytic and numerical results is addressed in more detail later in section 5.1.

3.1 Jet entropy

In this section we derive an expression for the entropy of a jet in terms of an integral over two subjet entropies, following [1]. To this end, we start by rewriting the jet density matrix $\rho = |\psi\rangle\langle\psi|$ in terms of basis vectors

$$\rho = \sum_{k,l,m,n} c_{kl} c_{mn} \, |\psi_k\rangle_R \langle\psi_m|_R \otimes |\psi_l\rangle_U \langle\psi_n|_U \,, \tag{3.1}$$

where $|\psi_m\rangle_R$ and $|\psi_m\rangle_U$ are bases for the resolved and unresolved subsystems respectively. The jet state, written in terms of these basis vectors, is just $|\psi\rangle = \sum_{m,n} c_{mn} \, |\psi_m\rangle_R \otimes |\psi_n\rangle_U$.

We then obtain the density matrix of the resolved subsystem by tracing out its unresolved complement in the following way:

$$\rho_R = \mathrm{tr}_U(\rho) = \sum_{k,l,m,n} c_{kl}c_{mn}\,|\psi_k\rangle_R\langle\psi_m|_R \times \mathrm{tr}\left(|\psi_l\rangle_U\langle\psi_n|_U\right). \tag{3.2}$$

If the density matrix of the subsystem R is diagonal in some basis $|b_m\rangle$, meaning that the measurements of b follow a classical probability distribution, then we say that the quantum number b has been *decohered*. As is argued in [1], the resolved subjets can be treated as hard parton states "dressed" with infrared and collinear particles which decohere the hard parton momenta. Thus, we get the following density matrix (dropping the subscript R from this point onward), where we also trace over spins:

$$\rho = \sum_{n=1}^{\infty}\int_H \mathrm{d}\Pi_n \frac{\mathrm{d}P}{\mathrm{d}\Pi_n}\,|p_1, p_2, ..., p_n\rangle\,\langle p_1, p_2, ..., p_n|\,, \tag{3.3}$$

where n is the number of hard partons, $\mathrm{d}P/\mathrm{d}\Pi_n$ is the normalized differential cross section (i.e. the "classical" probability distribution) of the jet and H indicates the hard region of phase space (i.e. the region above the cutoffs $z_{\min}$ and $R_{\min}$). The jet entropy is then defined as the Von Neumann entropy $\mathcal{S}$ of this density matrix:

$$\mathcal{S} = -\mathrm{tr}[\rho\ln\rho] = -\sum_{n=1}^{\infty}\int_H \mathrm{d}\Pi_n \frac{\mathrm{d}P}{\mathrm{d}\Pi_n}\ln\left(\frac{\mathrm{d}P}{\mathrm{d}\Pi_n}\Lambda^2\right), \tag{3.4}$$

where both the sum and the integral come from the trace operator. In order to make the probability $\mathrm{d}P/\mathrm{d}\Pi_n$ dimensionless, we were forced to introduce an arbitrary energy scale Λ^2 which converts the phase space element into a number of states $\mathrm{d}\Pi_n/\Lambda^2$. While Λ^2 cancels between the integration element and probability outside the logarithm in eq. 3.4, a factor is retained inside the logarithm. (The factor Λ^2 is introduced in agreement with [1].) Interestingly, Λ^2 does not drop out in the following calculations, and must be fixed somewhat arbitrarily in order to evaluate the entropy. A natural choice of Λ is introduced in the next section.

In order to turn eq. 3.4 into an expression involving the subjet entropies, we will factorize the phase space as follows:

$$\mathrm{d}\Pi_n\big(p_J\big) = \frac{p_\perp}{4\pi^2 z(1-z)}\,\mathrm{d}z\,\mathrm{d}p_\perp\,\mathrm{d}\Pi_m\big(zp_J + p_\perp\big)\,\mathrm{d}\Pi_{n-m}\big((1-z)p_J - p_\perp\big), \tag{3.5}$$

where p_J is the total jet momentum, which branches with transverse momentum $p_\perp$ and energy fraction z. Furthermore, using the splitting probability in section 2.2 and the phase space factorization in eq. 3.5 we get the factorized probability distribution:

$$\begin{aligned}\frac{\mathrm{d}P}{\mathrm{d}\Pi_n}(E,R) =& \frac{4\pi^2 z(1-z)}{p_\perp}\sum_{j,k}\frac{\alpha_s}{2\pi}\frac{P_{i\to jk}(z)}{p_\perp}e^{-\Gamma(R,p_\perp)} \\ &\times \frac{\mathrm{d}P}{\mathrm{d}\Pi_m}(zE,p_\perp)\,\frac{\mathrm{d}P}{\mathrm{d}\Pi_{n-m}}\big((1-z)E,p_\perp\big),\end{aligned} \tag{3.6}$$

where E is the total jet energy and R is the transverse momentum of the initial branching, which acts as an upper bound for subsequent splittings in the leading logarithmic approximation. In eq. 3.6 we have $i,j,k \in \{g,q,\bar{q}\}$, with i being the initial particle in the jet and j,k running over the various possible daughter particles. There is no sum over m in eq. 3.6 because we only consider the transverse momentum ordered branching. Instead, we will sum over m outside the phase space integral, integrating over the phase space region appropriate to each ordered branching. (A more detailed discussion regarding the sum over m can be found in [1].) Combining eqs. 3.4, 3.5 and 3.6 gives the desired equation for the entropy:

$$\begin{aligned}\mathcal{S}_i(E,R) = \mathcal{F}(E,R) + \int_{z_{\min}}^{z_{\max}}\mathrm{d}z\int_{R_{\min}}^{R}\mathrm{d}p_\perp\sum_{j,k}\frac{\alpha_s}{2\pi}\frac{P_{i\to jk}(z)}{p_\perp}e^{-\Gamma(R,p_\perp)} \\ \times\Big(\mathcal{S}_j(zE,p_\perp)+\mathcal{S}_k((1-z)E,p_\perp)\Big),\end{aligned} \tag{3.7}$$

$$\begin{aligned}\mathcal{F}(E,R) = \Gamma(R,R_{\min})e^{-\Gamma(R,R_{\min})} + \int_{z_{\min}}^{z_{\max}}\mathrm{d}z\int_{R_{\min}}^{R}\mathrm{d}p_\perp\sum_{j,k}\frac{\alpha_s}{2\pi}\frac{P_{i\to jk}(z)}{p_\perp}e^{-\Gamma(R,p_\perp)} \\ \times\left(\Gamma(R,p_\perp)-\ln\left(\frac{4\pi^2 z(1-z)}{p_\perp}\sum_{j,k}\frac{\alpha_s}{2\pi}\frac{P_{i\to jk}(z)}{p_\perp}\Lambda^2\right)\right),\end{aligned} \tag{3.8}$$

where we have used the the normalization

$$\sum_{n=1}^{\infty}\int d\Pi_n\,\frac{dP}{d\Pi_n} = 1, \tag{3.9}$$

and the identity $\sum_{n=2}^{\infty}\sum_{m=1}^{n-1}a_m b_{n-m} = \sum_{n=1}^{\infty}\sum_{m=1}^{\infty}a_n b_m$.[1] Note that in the case of a jet consisting of one single kind of particle, the entropy of the subjets will be similar to that of the parent jet. In this case, eq. 3.7 is an integral equation which might be solvable by analytic methods.

[1]The two sides of this identity are just the same sum shown with two different orders of summation. We can understand this visually by representing the terms $a_n b_m$ as points in a coordinate grid with one n-axis and one m-axis. The sum on the right hand side can then be seen as a sum over horizontal (or vertical) grid lines, while the left hand side is a sum over diagonal grid lines. In both cases we sum over the entire grid, so the two sums are equal (assuming appropriate convergence criteria).

3.2 The entropy of a gluon jet

In this section, we derive an expression for the entropy of a jet consisting only of gluons. The approach is to convert eq. 3.7 into an integro-differential equation that is solvable in the soft limit $z \ll 1$.

Inserting the soft limit of the gluon splitting function, $P_{g\to gg}(z) = 2C_A/z$, into eq. 2.12 and approximating $z_{\max} = (1 - z_{\min}) \approx 1$ gives the no-splitting probability

$$\Gamma(R, R_{\min}) = \frac{\alpha_s C_A}{\pi} \ln\left(\frac{E}{E_{\min}}\right) \ln\left(\frac{R}{R_{\min}}\right). \tag{3.10}$$

After multiplying eq. 3.7 by the inverse Sudakov factor $\exp(\Gamma(R, R_{\min}))$ and differentiating, we then get

$$R\,\frac{\partial \mathcal{S}}{\partial R}(E, R) = R\, e^{-\Gamma(R,R_{\min})} \frac{\partial}{\partial R}\left(e^{\Gamma(R,R_{\min})}\mathcal{F}\right) + \int_{z_{\min}}^{1} \frac{\mathrm{d}z}{z}\,\frac{\alpha_s C_A}{\pi}\mathcal{S}(zE, R), \tag{3.11}$$

where we have used the soft approximation $(1 - z) \approx 1$ and the unitarity condition

$$\int_{z_{\min}}^{z_{\max}} \mathrm{d}z \int_{R_{\min}}^{R} \mathrm{d}p_\perp \frac{P_{i\to jk}}{p_\perp} e^{-\Gamma(R,p_\perp)} = 1 - e^{-\Gamma(R,R_{\min})}. \tag{3.12}$$

An equation similar to eq. 3.11 appears in [1]. However, that equation is derived assuming the branchings are ordered by emission angle instead of transverse momentum. This changes the form of $\mathcal{F}$ (eq. 3.8), which appears in the inhomogeneous term. More specifically, in our case the z-dependent factor inside the logarithm in $\mathcal{F}$ is $z(1 - z)P_{g\to gg}(z)$, which is approximately constant in the soft limit. (The z-dependence cancels because we have $(1 - z) \approx 1$ and $P_{g\to gg}(z) \propto 1/z$ in the soft limit.) When angular ordering is assumed however, this z-dependence does not disappear, as can be seen in [1]. We rederived the analytic entropy for angular ordering using the approach shown below, and found that the z-dependence inside the logarithm added several complications compared to the present derivation. However, it should be noted that the final results still have a surprisingly similar functional form.

Now, we solve eq. 3.11. First, suppose there is a power series solution $s_0(\Gamma)$ to the homogeneous part of the equation. It is straightforward to solve for the coefficients of this series, giving a solution which we rewrite in terms of a modified Bessel function of the first kind:

$$s_0(\Gamma) = I_0(x) = \sum_{m=0}^{\infty} \frac{1}{(m!)^2}\left(\frac{x}{2}\right)^{2m}, \tag{3.13}$$

$$x(E, R) \equiv 2\left(\frac{\alpha_s C_A}{\pi} \ln\frac{E}{E_{\min}} \ln\frac{R}{R_{\min}}\right)^{1/2}, \tag{3.14}$$

where x is related to Γ by $\Gamma = x^2/2$. In order to find an inhomogeneous solution, we first compute the inhomogeneous term in eq. 3.11 explicitly, and note that it would be cancelled by the addition of a term $f = 2\ln(R/R_{\min}) + \mathrm{c}$ in the solution, where c is a function of $z_{\min}$ and $R_{\min}$. However, the term c would have unnatural singularities such as $z_{\min} = 1$, meaning that the entropy would diverge as the jet becomes less resolved. Instead, one can search for a product solution $fs_1(\Gamma)$ where s_1 is a power series, which gives another modified Bessel function

$$s_1(\Gamma) + 1 = \frac{2}{x} I_1(x(E,R)) = \sum_{m=0}^{\infty} \frac{1}{(m!)^2(m+1)} \left(\frac{x}{2}\right)^{2m}. \tag{3.15}$$

Combining these results gives the expression for the entropy:

$$\mathcal{S}(E,R) = \left(1 + \ln\left(\frac{R_{\min}^2}{4\pi C_A \alpha_s \Lambda^2}\right)\right)\big(I_0(x) - 1\big) + 2\ln\frac{R}{R_{\min}}\left(\frac{2}{x} I_1(x) - 1\right), \tag{3.16}$$

where the energy dependence comes through the variable $x(E,R)$ (eq. 3.14). Eq. 3.16 suggests a natural choice of energy scale $\Lambda^2 = 4\pi C_A \alpha_s / R_{\min}^2$ (assuming constant α_s), which removes the color-factor-dependent logarithm.

4 Numerical method

An event generator is a program that simulates collision events. For this project, we devised a simple event generator, based on [2], which creates parton jets and calculates their entropy. Importantly, we include recoil in our event generator, and investigate how this affects the entropy calculations. First, in section 4.1 we discuss some key features of our specific event generator implementation, which are explained in more detail in [10] and [11]. Then, in section 4.2 we give an explanation of the important veto algorithm. The numerical results are presented later, in sections 5.1 and 5.2.

4.1 The event generator

We developed our event generator based on [2], modifying and adding to this code in order to use it to calculate jet entropy. As part of this process we made modifications to the jet clustering algorithm, wrote a new function for setting up the initial state and wrote a program that uses the branching history of a jet to calculate its entropy. Understanding, creating and modifying the various pieces of code used in the event generator constituted a large part of the effort put into this project. Initially, the event generator constructs two on-shell partons in the center-of-mass frame, and subsequent splittings are then proposed and accepted/rejected according to the veto algorithm (section 4.2). Once a splitting is accepted, the new on-shell particles are added to the current state of the event and the process repeats until the transverse momentum reaches a minimum threshold. Finally, a

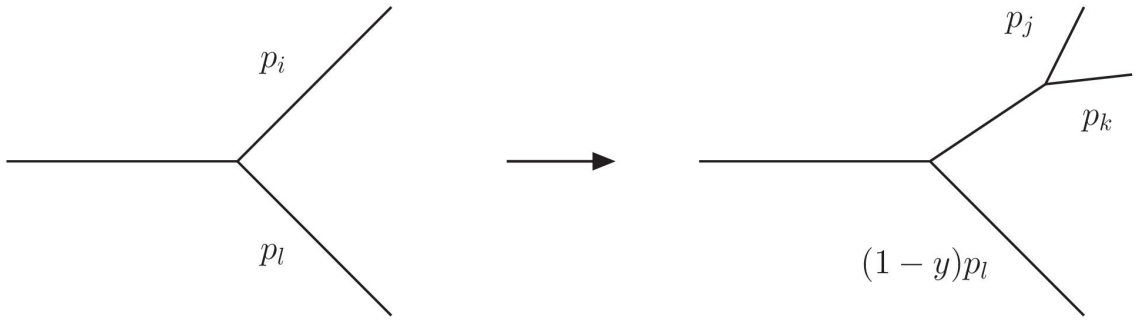

Figure 3: A splitting of an on-shell particle p_i allowed by the inclusion of recoil. A fraction y of the spectator momentum p_l is added to the daughter momenta p_j and p_k, which allows all particles to stay on-shell while also conserving four-momentum.

branching history is created using a jet algorithm. Some key properties of our implementation are:

Recoil - All particles in the event are kept on-shell, so naively they cannot branch without violating four-momentum conservation. This issue is resolved by assigning a recoiling particle to each branching. When a splitting occurs, a fraction y of the recoil momentum p_l is distributed among the daughter particles as follows:

$$p_j = zp_i + (1-z)yp_l + p_\perp \tag{4.1}$$
$$p_k = (1-z)p_i + zyp_l - p_\perp \tag{4.2}$$

where the recoil fraction y is determined by the on-shell condition $p_j^2 = p_k^2 = 0$, which gives $y = p_\perp^2/2z(1-z)p_ip_l$. At the same time, the recoiler momentum is rescaled to $(1-y)p_l$, which keeps the total momentum of the event constant. Thus, we produce a $2 \to 3$ branching where all particles are kept on-shell and momentum is conserved (see Fig. 3). To generate such branchings we use the Catani-Seymour splitting functions [12], which are suitable for splittings that include recoil:

$$P_{q\to qg}(z,y) = C_F\left(\frac{2}{1-z(1-y)} - (1+z)\right), \tag{4.3}$$
$$P_{g\to gg}(z,y) = 2C_A\left(\frac{1}{1-(1-z)(1-y)} + \frac{1}{1-z(1-y)} - 2 + z(1-z)\right), \tag{4.4}$$
$$P_{g\to qq}(z,y) = T_R\Big(1 - 2z(1-z)\Big). \tag{4.5}$$

The large N_C limit - The treatment of color in an $SU(N_C)$ gauge theory simplifies when the gauge group is replaced by $U(N_C)$. This is because the number of gluons in the $U(N_C)$ theory equals the number of two-color combinations (N_C^2), which enables a description based on "color-flow" [13]. In this description, gluons are represented by two parallel diagram lines, each of which is associated with a specific color, and quarks are

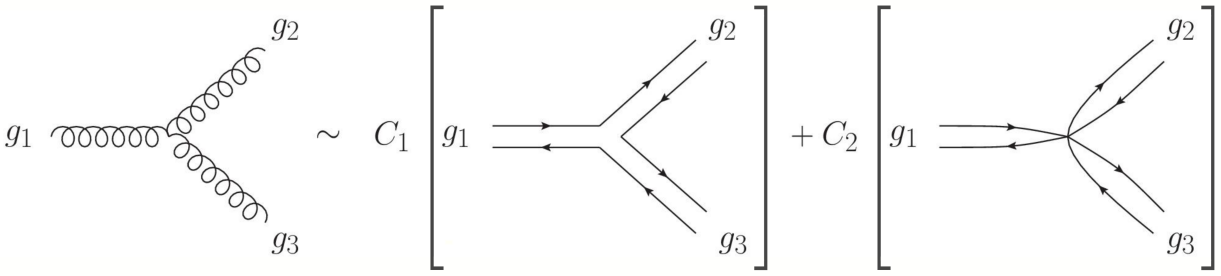

Figure 4: The $g \to gg$ vertex written as a linear combination of two color-flow diagrams, where C_1 and C_2 are constant coefficients. Right pointing arrows indicate the flow of color-indices, while left-pointing arrows show the flow of anti-color indices. We choose the planar color-flow diagram on the left to set the colors of the emission and radiator after a splitting.

represented by a single such line. When radiating from a fixed color line, we define a color-connected recoiler and choose the planar color-flow (see Fig. 4) to set the colors of the daughter particles after the branching. The change of gauge group is justified by [14], which shows that the ghost gluon (i.e. the gluon that was introduced by the change of gauge group) is suppressed by powers of $1/N_C$ and only couples to quarks.

The Durham Algorithm - Once an event has been generated, we construct a branching history using the Durham algorithm [15]. This is done by repeatedly recombining the pairs of particles with the smallest value of

$$y_{jk} = \frac{p_\perp^2}{Q^2}, \tag{4.6}$$

where Q^2 is the invariant mass of the event. Here, $p_\perp^2$ is computed using

$$p_\perp^2 \approx z(1-z)(p_j + p_k)^2 \approx 2\min(E_j^2, E_k^2)(1 - \cos\theta_{jk}), \tag{4.7}$$

where the first approximation follows from eq. A.5 and the second approximation follows from $z^2(1-z)^2 \approx \min(z^2, (1-z)^2)$. In our case, we simply take the momentum of the parent particle to be $p_j + p_k$, although more complicated recombination schemes are possible. (Examples of different recombination schemes can be found in [12].)

In order to compute the entropy of a given jet, we use the equation

$$\begin{aligned} s = {} & \Gamma(R, R_{\min}, z_{\max}, z_{\min}) \\ & + \sum_{n=1}^{N} \left(\Gamma(p_{\perp n}, R_{\min}, z_n, z_{\min}) - \ln\left(\frac{4\pi^2 z_n(1-z_n)}{p_{\perp n}} \sum_{j,k} \frac{\alpha_s}{2\pi} \frac{P_{i\to jk}(z_n)}{p_{\perp n}} \Lambda^2 \right) \right), \end{aligned} \tag{4.8}$$

which is obtained by changing the evolution parameter of an equation presented in [1]. Here, we sum over every splitting in the branching history, with $p_{\perp n}$ and z_n being the transverse momentum and energy fraction of the n'th splitting. Note that the last two arguments of Γ are just the integration limits of z in eq. 2.12, which were previously omitted as explicit variables in order to simplify notation. In accordance with what is said for angular ordering in [1], eq. 4.8 will reproduce the general integral equation for jet entropy (eq. 3.7) when averaged over many events.

4.2 The veto algorithm

In order to generate a jet we will need to sample from the probability distribution in eq. 2.14. This will be done using the veto algorithm, which we describe presently. This description is based on the more detailed treatment found in [7].

Sampling from a probability distribution f is straightforward if the anti-derivative F is easily invertible. In this case, a variable x is generated from a uniformly distributed variable $R \in [0,1]$ according to the standard formula

$$x = F^{-1}\left((F(x_{\max}) - F(x_{\min}))R + F(x_{\min})\right). \tag{4.9}$$

However, if f does not have a simple anti-derivative then one can first generate x from a function $g > f$, where g has an easily invertible anti-derivative G. We then introduce the accept/reject criterion $f(x)/g(x) < R_1$, where $R_1 \in [0,1]$ is uniformly distributed. This gives the desired sampling probability $g(x) \cdot (f(x)/g(x)) = f(x)$. Now, consider the distribution

$$\mathcal{P}_f(x) = f(x) \exp\left\{ - \int_0^x \mathrm{d}x' f(x') \right\}, \tag{4.10}$$

which is of the same form as eq. 2.14. If F is known, then the anti-derivative of $\mathcal{P}_f$ can be computed explicitly, giving

$$x = F^{-1}\left(F(0) + \ln R\right), \tag{4.11}$$

which is the equivalent of eq. 4.9 for $\mathcal{P}_f$. However, the accept/reject condition $f(x)/g(x) < R$ cannot be generalized naively. Instead, one employs the veto algorithm, described in Fig. 5. The key feature of the veto algorithm is that any proposed sample x_i must be greater than the previous rejected sample x_{i-1}. Thus, every accepted sample x is preceded by an increasing sequence of rejected samples $x_1 < x_2 < ... < x_n$. The probability of the i'th sample being rejected is

$$\mathcal{P}^i_{\text{rejected}}(x_i) = \exp\left\{ \int_{x_{i-1}}^{x_i} \mathrm{d}x' g(x') \right\} g(x_i) \left(1 - \frac{f(x_i)}{g(x_i)}\right), \tag{4.12}$$

where the exponential factor is the probability that no sample was generated in the range $x_{i-1} < x < x_i$ (which follows from the same logic used in section 2.2), $g(x_i)$ is the probability of generating x_i and the rightmost factor is the probability that x_i is rejected. The

probability of x_i being accepted is obtained by changing $(1 - f/g)$ to f/g in eq. 4.12. Thus, the probability of rejecting n samples before accepting the sample x is

$$\begin{aligned}\mathcal{P}_f^n(x) = &\exp\left\{-\int_{x_n}^{x} \mathrm{d}x' g(x')\right\} g(x)\frac{f(x)}{g(x)} \\ &\times \int_0^x \mathrm{d}x_1 \int_{x_1}^x \mathrm{d}x_2 \ldots \int_{x_{n-1}}^x \mathrm{d}x_n \prod_{i=1}^{n} \exp\left\{-\int_{x_{i-1}}^{x_i} \mathrm{d}x' g(x')\right\} g(x_i)\left(1 - \frac{f(x_i)}{g(x_i)}\right),\end{aligned} \tag{4.13}$$

where the first line gives the probability that x is accepted and the second line integrates the rejection probabilities over all the possible sequences of n rejected samples. Note that after multiplying the exponentials the remaining integral is unchanged by permutations of the x_i's. Taking the average of all the permutations separates the integrals, giving

$$\mathcal{P}_f^n(x) = f(x)\exp\left\{-\int_0^x \mathrm{d}x' g(x')\right\}\frac{1}{(n-1)!}\left(\int_0^x \mathrm{d}x'(g(x') - f(x'))\right)^n. \tag{4.14}$$

It is now clear that

$$\mathcal{P}_f^{\text{veto}}(x) = \sum_{n=0}^{\infty} \mathcal{P}_f^n = f(x)\exp\left\{-\int_0^x \mathrm{d}x' f(x')\right\}, \tag{4.15}$$

which is the desired probability distribution.

5 Numerical results

The numerical results are divided into two sections. First, in section 5.1 we show the transverse momentum distribution and entropy of gluon jets. Then, in section 5.2 we discuss possible graviton splitting kernels and show how these kernels affect the jet properties.

5.1 QCD

In Fig. 6 we compare the numerical and analytic entropy calculations, and find that the numerical entropy curve deviates from the analytic curve at high resolutions. Such a deviation is not seen in [1], where recoil is ignored. It thus appears that the inclusion of recoil significantly affects the behaviour of the entropy. In fact, it appears that the effect of including recoil is comparable to having a running coupling constant, which was investigated by Neill and Waalewijn. It should be clarified, that the deviation between the analytic and numerical results does not imply that there are errors in the numerics. This is because the analytic calculation makes rough assumptions about the phase space boundaries by treating $p_\perp$ and z as independent variables, while in reality a given value of $p_\perp$ puts restrictions on the possible values of z through eq. A.5. It appears that the event

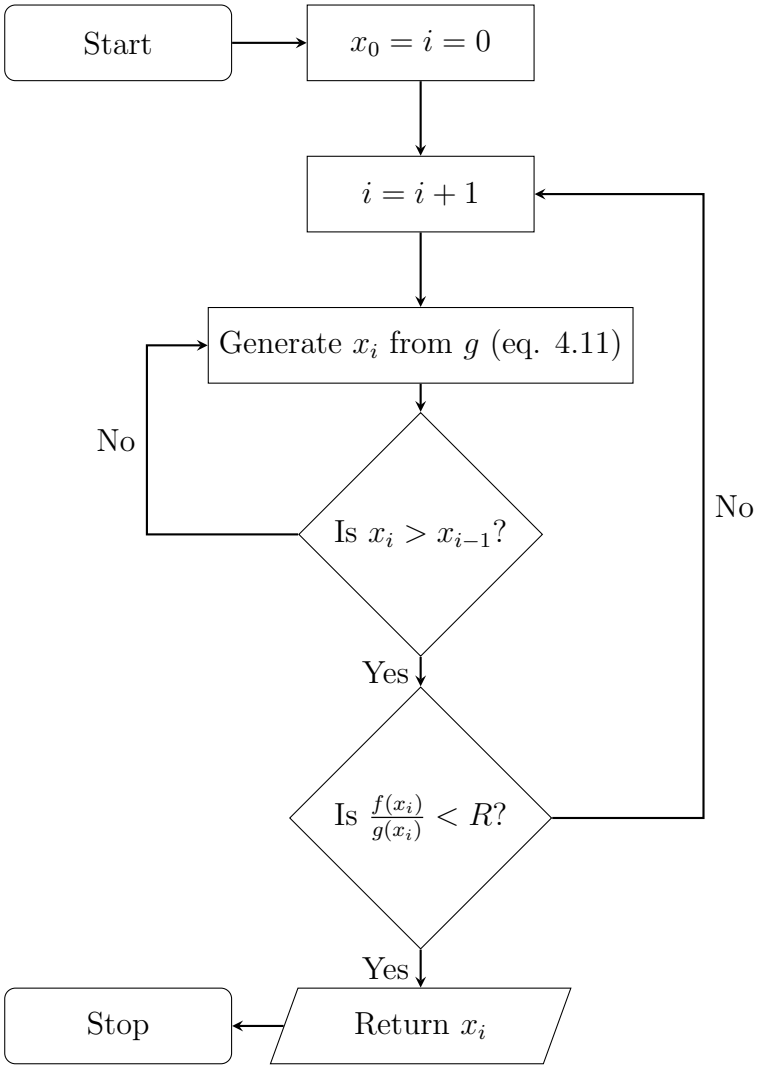

Figure 5: An overview of the veto algorithm. Here, a sample x is generated from the probability distribution $\mathcal{P}_f$ (eq. 4.10). The function g is an overestimate of f.

generator used by Neill and Waalewijn does not not enforce these phase space restrictions due the way in which they avoid recoil, so it is perhaps not surprising that the analytic and numerical results are in stronger agreement when recoil is ignored.

As was mentioned in section 4, our event generator creates two distinct jets per event. We investigated whether the results have been influenced by the transfer of momentum between these jets through recoil. This was done by suppressing high recoil splittings, which in turn should reduce the interaction between the jets. For this purpose, we introduced the splitting function

$$P_{g\to gg}(z,y) = 2C_A\left(\frac{z(1-y)}{1-z(1-y)} + \frac{(1-z)(1-y)}{1-(1-z)(1-y)} + z(1-z)(1-y)^2\right), \qquad (5.1)$$

where y is the recoil fraction defined in section 4.1. This equation is obtained by re-arranging the terms in eq. 4.4 and introducing extra factors $(1-y)$ in the numerators. Suppressing recoil should slightly suppress large transverse momenta, which leads to fewer resolved states and thus a smaller overall entropy. However, despite the smaller magnitude, the suppressed entropy curve shows a similar behaviour to the non-suppressed curve at high resolutions. This suggest that the behaviour at high resolution is not caused by momentum transfer between jets alone.

The distribution of transverse momentum at different stages of branching is shown in Fig. 7. As expected, the general shape of the distribution matches the prediction of a divergent splitting probability $\mathcal{P}_{i\to jk} \propto 1/p_\perp$ which is suppressed by the Sudakov form factor at small transverse momenta. We can tell from the ratio plot at $2 \to 3$ jet resolution that the jet with suppressed recoil tends to have very slightly more splittings at small transverse momenta. This is reasonable because favouring low recoils should give smaller transverse momenta through the relation $p_\perp^2 = z(1-z)yp_ip_l$. When the initial splitting has low transverse momentum, the jet will tend to have fewer resolvable splittings due to ordering, so this could account for the difference between the numerical entropies in Fig. 6.

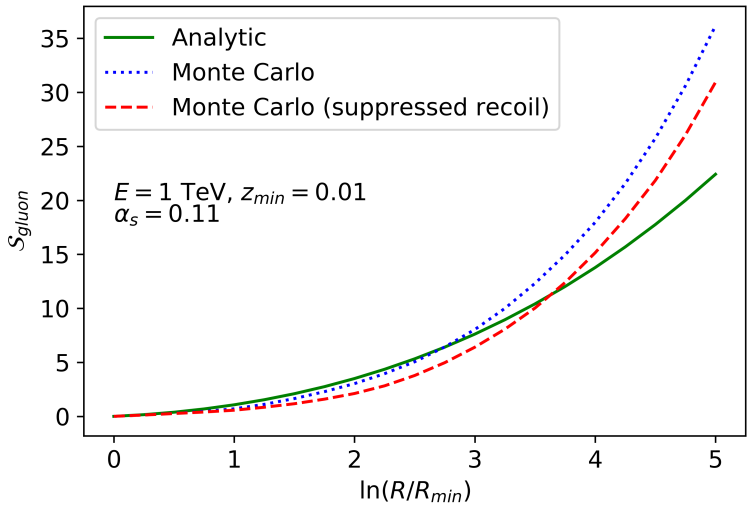

Figure 6: A comparison of the numerical gluon entropy at fixed coupling and the analytical calculation. The dashed curve is generated taking eq. 5.1 as the splitting function. The entropy was also calculated using the small z limit of the splitting functions, but this did not significantly affect the final result.

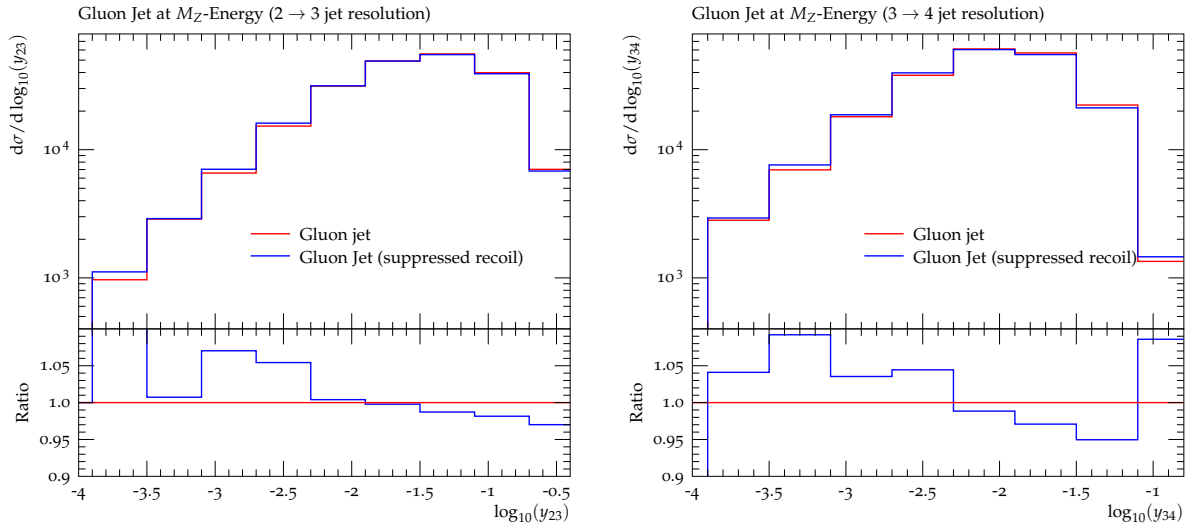

Figure 7: The distribution of transverse momenta at $2 \to 3$ and $3 \to 4$ jet resolution, collected from 10,000 events. The jet energy is $M_Z \approx 91.1876$ GeV, the lower $p_\perp$ cutoff is 1 GeV and the coupling is fixed at $\alpha_s = 0.11$. The lower plot in each figure shows the ratio between the histograms.

5.2 Gravity

In section 2.1 we remarked that virtual diagrams have to be included in the cross section of a splitting process before we can properly define the corresponding splitting function. In particular, we mentioned that virtual contributions give rise to the (+)-prescription, defined by

$$(f(x))_+ = \lim_{\varepsilon\to 0}\left[\Theta(1-x-\varepsilon)f(x) - \delta(1-x)\int_0^{1-\varepsilon} \mathrm{d}y f(y)\right], \tag{5.2}$$

which removes infrared singularities. Here, Θ is the standard step-function. Notably, in QCD the (+)-prescription is applied to divergent parts of the splitting function, possibly leaving a non-divergent term called a collinear piece. For gravity, where collinear singularities are suppressed by the presence of momentum factors in the vertices [3], there are no hard collinear pieces in the splitting function. Thus, we propose several graviton splitting kernels by removing non-divergent terms from the corresponding splitting kernels in QCD. We can immediately obtain one candidate for the (graviton $\to$ graviton + graviton) splitting function by removing the last two terms in eq. 4.4, giving

$$P_1(z,y) = \frac{1}{1-(1-z)(1-y)} + \frac{1}{1-z(1-y)}. \tag{5.3}$$

Here, we have removed the negative collinear piece $z(1-z)-2$. Similarly, we can rewrite eq. 4.4 and remove a positive collinear piece, which gives the graviton splitting function

$$P_2(z,y) = \frac{1-z}{1-(1-z)(1-y)} + \frac{z}{1-z(1-y)}, \tag{5.4}$$

where we have removed the term $z(1-z)$ and terms suppressed by powers of y. Finally, as in section 5.1, we test the effect of a splitting function which suppresses high recoils

$$P_3(z,y) = \frac{(1-z)(1-y)}{1-(1-z)(1-y)} + \frac{z(1-y)}{1-z(1-y)}, \tag{5.5}$$

which is just $(1-y)P_2$. The average entropies of the different "graviton" jets are shown in Fig. 8. We observed that the entropy mainly depends on the branching properties of the jet. That is, changing the Sudakov terms in eq. 4.8 does not significantly affect the results. It was also noted that the relative magnitudes of the entropy curves are correlated with the total number of emissions in the jet event. This is reasonable, since [1] found the particle multiplicity to be closely related to the jet entropy. (For one, they share the same asymptotic behaviour.) It does then look probable that the difference in multiplicity between the jets accounts for a large part of the discrepancy between the entropy curves. In Fig. 9 we show how the graviton splitting functions affect the transverse momentum distributions. The main conclusion drawn from the figures below is that the change in splitting function has a large impact on the entropy.

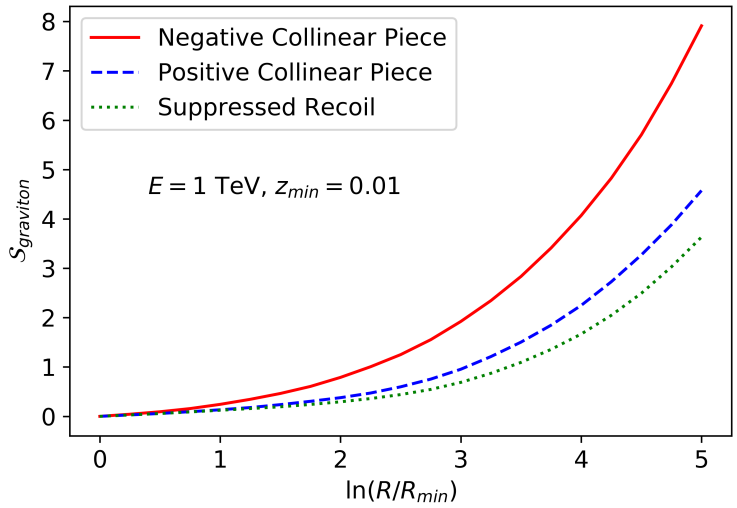

Figure 8: The jet entropies corresponding to different graviton splitting functions. The solid line is generated using eq. 5.3, the dashed line is generated using eq. 5.4 and the dotted line is generated using eq. 5.5.

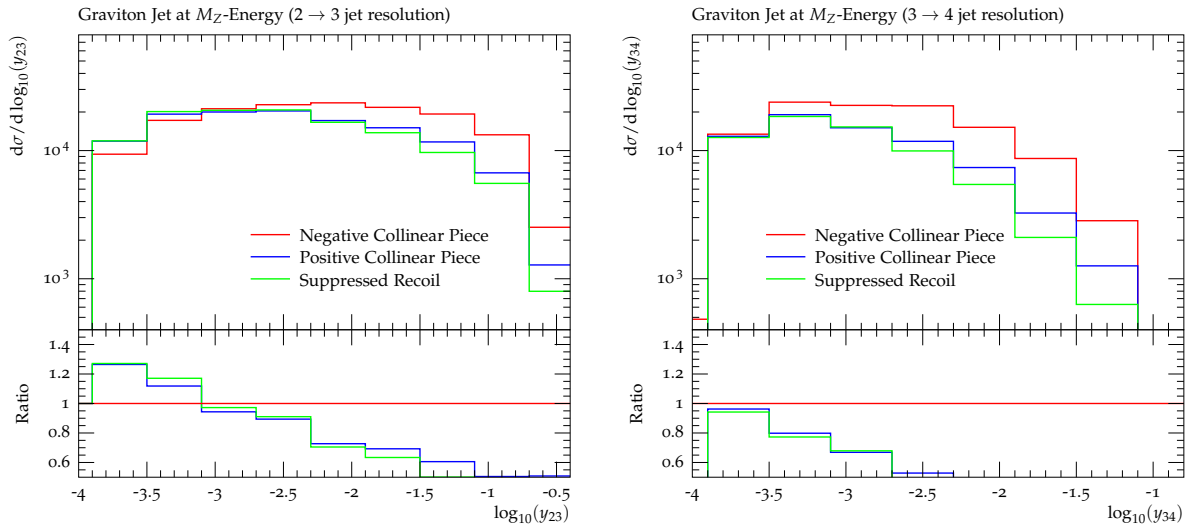

Figure 9: Transverse momentum distributions for the various graviton splitting functions, at $2 \to 3$ and $3 \to 4$ jet resolution. The data is collected from 10,000 events at M_Z-energy, with a lower $p_\perp$ cutoff of 1 GeV. The negative collinear-, positive collinear- and recoil suppression histograms are generated using the splitting functions in eqs. 5.3, 5.4 and 5.5 respectively.

6 Conclusions and further work

In this thesis we have found that the entropy of a numerical jet depends strongly on whether recoil is included in the event generator. This was determined by finding a significant deviation between numerical and analytic entropy calculations when recoil is included, which does not occur when recoil is neglected [1]. To find this result, a simple event generator was developed, and an analytic expression for the entropy of a jet was derived. A natural continuation of this work is to test whether jet entropy varies significantly between various other recoil prescriptions. The fact that our jet entropy behaved very differently from that in [1] suggests that this could be the case. If so, it would be interesting to investigate which recoil prescriptions give the best agreement with experimental jet entropy.

We have also investigated three models of graviton splitting kernels, which where constructed by removing collinear pieces from the gluon splitting functions. We found that the resulting "graviton" jet entropy depends significantly on which collinear piece was removed. This work can be naturally continued by attempting to derive more accurate graviton splitting kernels and writing a more sophisticated event generator that does not simply approximate graviton interactions as gluon interactions.

A Momentum parameterization

In a final-state splitting, like that seen in Fig. 1, the initial particle must have a non-negative virtuality (assuming the "mostly minuses" spacetime signature).[2] This is accommodated by the following momentum parameterization, where the momenta are labeled as in Fig. 1:

$$p_i = \left(E + \frac{p_\perp^2}{2z(1-z)E}, 0, 0, E\right), \tag{A.1}$$

$$p_j = \left((1-z)E + \frac{p_\perp^2}{4z(1-z)E}, 0, 0, (1-z)E + \frac{p_\perp^2(1-2z)}{4z(1-z)E}\right) + p_\perp, \tag{A.2}$$

$$p_k = \left(zE + \frac{p_\perp^2}{4z(1-z)E}, 0, 0, zE - \frac{p_\perp^2(1-2z)}{4z(1-z)E}\right) - p_\perp. \tag{A.3}$$

Here, the parameter $p_\perp$ is the transverse momentum of the splitting. That is, $p_\perp$ is the component of p_j that is transverse to p_i. The parameters E and z are the energy and energy fraction of the splitting respectively. This momentum parameterization can be derived by requiring the the spatial component of p_i to be constant with respect to $p_\perp$ and

[2] This can be seen directly from the relation $p_i^2 = (p_j + p_k)^2 = 2E_jE_k(1-\cos\theta) \geq 0$, where θ is the angle between the spatial components of p_j and p_k, and E_j and E_k are the energies of the daughter particles. In the second equality we used the fact that the daughters are on-shell and (approximately) massless.

putting the outgoing momenta on-shell. In other words, upon fixing the form of p_i the parameterization is unique. In this decomposition we have

$$p_j^2 = p_k^2 = 0 + \mathcal{O}(p_\perp^4), \tag{A.4}$$

$$p_i^2 = \frac{p_\perp^2}{z(1-z)} + \mathcal{O}(p_\perp^4). \tag{A.5}$$

References

[1] Duff Neill and Wouter J. Waalewijn. Entropy of a Jet. *Phys. Rev. Lett.*, 123(14):142001, 2019.

[2] Tutorial on parton showers. https://www.slac.stanford.edu/ shoeche/cteq15/ws/PS.pdf. Accessed: 2020-06-29.

[3] Steven Weinberg. Infrared photons and gravitons. *Phys. Rev.*, 140:B516–B524, 1965.

[4] T. Kinoshita. Mass singularities of Feynman amplitudes. *J. Math. Phys.*, 3:650–677, 1962.

[5] M. Bohm, Ansgar Denner, and H. Joos. *Gauge theories of the strong and electroweak interaction*. Teubner, 2001.

[6] Guido Altarelli and G. Parisi. Asymptotic Freedom in Parton Language. *Nucl. Phys. B*, 126:298–318, 1977.

[7] Torbjorn Sjostrand, Stephen Mrenna, and Peter Z. Skands. PYTHIA 6.4 Physics and Manual. *JHEP*, 05:026, 2006.

[8] V.V. Sudakov. Vertex parts at very high-energies in quantum electrodynamics. *Sov. Phys. JETP*, 3:65–71, 1956.

[9] R. K. Ellis, W. J. Stirling, and B. R. Webber. *Parton branching and jet simulation*, page 157–192. Cambridge Monographs on Particle Physics, Nuclear Physics and Cosmology. Cambridge University Press, 1996.

[10] Stefan Höche. Introduction to parton-shower event generators. In *Theoretical Advanced Study Institute in Elementary Particle Physics: Journeys Through the Precision Frontier: Amplitudes for Colliders*, pages 235–295, 2015.

[11] Stefan Höche and Stefan Prestel. The midpoint between dipole and parton showers. *European Physical Journal C. Particles and Fields*, 75(9), 9 2015.

[12] S. Catani and M.H. Seymour. A General algorithm for calculating jet cross-sections in NLO QCD. *Nucl. Phys. B*, 485:291–419, 1997. [Erratum: Nucl.Phys.B 510, 503–504 (1998)].

[13] W. Kilian, T. Ohl, J. Reuter, and C. Speckner. QCD in the Color-Flow Representation. *JHEP*, 10:022, 2012.

[14] Gerard 't Hooft. A Planar Diagram Theory for Strong Interactions. *Nucl. Phys. B*, 72:461, 1974.

[15] S. Catani, Yuri L. Dokshitzer, M. Olsson, G. Turnock, and B.R. Webber. New clustering algorithm for multi - jet cross-sections in e+ e- annihilation. *Phys. Lett. B*, 269:432–438, 1991.